Ambiguity Function for SONAR

J. M. Moura

LASIP, Deprt. Elect. Comp. Eng.
Carnegie Mellon University
Pittsbugh, PA 15213, USA

M. J. Rendas

CAPS, Dep. Eng. Elect. Comp.
Inst. Superior Técnico
1906 Lisboa Codex, Portugal

Abstract

We pesent a new definition of ambiguity and illustrate its aplication to the study of passive localization of sources in deep ocean situations. The tool developed alllows the study of the impact of all relevant parameters, those relative to the physical medium, as well as those pertinent to the instrumentation and signals involved. In the study reported here, particular attention is given to factors as source signal bandwidth and array size and location. The potential impact of a modelisation of the temporal (inter-arrival) structure has been demonstrated.

1 Introduction

In radar, the ambiguity function introduced by Woodward plays a significant role in target localization. Woodward's context is that of active systems where the received signal is a delayed replica of the transmitted signal possibly corrupted by additive noise. The signal has known characteristics. The sonar environment is less friendly, introducing additional difficulties and distortions. In particular, non-homogeneities of the propagation channel, as well as the channel boundaries, give rise to multiple paths. Further, in passive sonar, the signal is radiated by the source, hence its characteristics and parameters are unknown to the receiver.

The present paper addresses the problem of defining the ambiguity function in such a way that it accounts for the multipath present in the sonar problem and that it handles signals whose structure is not completely known to the receiver. The ambiguity function herein described generalizes the ambiguity introduced by Woodward. The paper illustrates the definition of ambiguity for deep ocean scenarios. We pay particular attention to how the ambiguity structure varies with the array location, the array size, and the radiated signal bandwidth. To assess the importance of multipath modeling on the observability structure, we compare the ambiguity surfaces to those obtained with propagation models that consider only the spatial structure (wavefront curvature and orientation) of the received wavefield.

2 Ambiguity Function

Consider that the observations' power spectrum is described by

$$R_\theta(\omega) = \mathcal{S}(\omega) h_\theta(\omega) h_\theta(\omega)^H + \sigma^2(\omega) I_K$$

where we assume that the observation noise is spatially incoherent, with known power density $\sigma^2(\omega)$. In the previous equation, $\mathcal{S}(\omega)$ is the *unknown* source spectral density and $h_\theta(\omega)$ is the resultant vector, that describes the coherent combination of the steering vectors corresponding to the P replicas received.

The resultant vector can be decomposed as

$$h_\theta(\omega) = D(\theta) b(\theta)$$

where the $K \times P$ matrix $D(\theta)$ describes the spatial structure of the individual replicas, depending only on the inter-sensor delays for each received path, and $b(\theta)$ is a P dimensional vector that depends only on their temporal alignment.

A. Complete Model

When a complete model of the channel is used, the resultant vector is perfectly known for each θ, i.e., both the matrix $D(\theta)$ and the vector $b(\theta)$ in the previous equation are known functions of the source location θ.

In this case, application of the definition of ambiguity introduced in [1, 2] yields the following expression for the ambiguity between scanning location θ, and a source at the true location θ_0 radiating a signal with

1058-6393/92 $03.00 © 1992 IEEE

spectrum $S_0(\omega)$, see [2]:

$$\mathcal{A}(\theta_0,\theta)^{spa/tim}_{\mathcal{S}_0} = \int \frac{\mathrm{SNR}(\omega)}{\int \mathrm{SNR}(\omega)d\omega}\mathcal{A}(\theta_0,\theta)^{(c)}_{\mathcal{S}_0} - \frac{1}{\int \mathrm{SNR}(\omega)d\omega}\ln\frac{1+\mathrm{SNR}(\omega)\mathcal{A}(\theta_0,\theta)^{(c)}_{\mathcal{S}_0}}{1+\mathrm{SNR}(\omega)}d\omega \quad (1)$$

where $\mathrm{SNR}(\omega)$ is the ratio of *received* signal to noise power,

$$\mathrm{SNR}(\omega) \triangleq \frac{\mathcal{S}_0(\omega)\|h_{\theta_0}(\omega)\|^2}{\sigma^2(\omega)}, \quad (2)$$

and $\mathcal{A}(\theta_0,\theta)^{(c)}_{\mathcal{S}_0}$ is the analogue of the classical ambiguity function, i.e., the square of the cosine of the angle between the resultant vectors for the two values of source location.

$$\mathcal{A}(\theta_0,\theta)^{(c)}_{\mathcal{S}_0} \triangleq \frac{|h_{\theta_0}(\omega)^H h_\theta(\omega)|^2}{\|h_\theta(\omega)\|^2\|h_{\theta_0}(\omega)\|^2}.$$

Note that this function can be written using the orthogonal projection operator onto the (one-dimensional) space spanned by the vector $h_\theta(\omega)$:

$$\mathcal{A}(\theta_0,\theta)^{(c)}_{\mathcal{S}_0} = \frac{\left\|\Pi_{h_\theta(\omega)}\left[h_{\theta_0}(\omega)\right]\right\|^2}{\|h_{\theta_0}(\omega)\|^2}$$

B. Spatial Modeling

When the *spatial model* is used, $b(\theta)$ is modeled as an unknown deterministic vector, $b(\omega)$, and the spectral density of the observations has the following form:

$$\mathcal{R}_\theta(\omega) = \sigma^2(\omega)I + \mathcal{S}(\omega)D(\theta)b(\omega)b(\omega)^H D(\theta)^H$$

Simultaneous lack of knowledge of $\mathcal{S}(\omega)$ and $b(\omega)$ implies that only the product $\sqrt{\mathcal{S}(\omega)}b(\omega)$ can be determined, i.e., the only restriction on the noiseless component of $\mathcal{R}_\theta(\omega)$ is that it has rank one, meaning that all the replicas are perfectly correlated. This increased uncertainty leads to [2] the following expression for the ambiguity

$$\mathcal{A}(\theta_0,\theta)^{sp}_{b_0} = \int \frac{\mathrm{SNR}(\omega)}{\int \mathrm{SNR}(\omega)d\omega}\left[\mathcal{A}(\theta_0,\theta)^{(d)}_{b_0} - \frac{1}{\mathrm{SNR}(\omega)}\ln\frac{1+\mathrm{SNR}(\omega)\mathcal{A}(\theta_0,\theta)^{(d)}_{b_0}}{1+\mathrm{SNR}(\omega)}\right]d\omega \quad (3)$$

where $\mathrm{SNR}(\omega)$ is defined by eq. (2), and

$$\mathcal{A}(\theta_0,\theta)^{(d)}_{b_0} \triangleq \frac{\left\|\Pi_{\mathcal{H}(\theta)}D(\theta_0)b_0\right\|^2}{\|D(\theta_0)b_0\|^2},$$

and $\Pi_{\mathcal{H}(\theta)}$ denotes the orthogonal projection operator into the subspace $\mathcal{H}(\theta)$, generated by the P steering vectors (columns of the matrix $D(\theta)$) that correspond to the scanning location θ.

Note that in this case the one dimensional vector $h_\theta(\omega)$ is replaced by the P-dimensional subspace spanned by the individual steering vectors. This fact is an immediate consequence of having a larger number of degrees of freedom on the model that is being fitted to the observations.

3 Spatial/Temporal Modeling

In this section we present ambiguity surfaces computed using the definition given in the previous section.

We consider a deep ocean area (bottom depth is 5 Km), and a bilinear velocity profile. Duct axis is located 914 meters below surface. We assume a negative velociy gradient of $-.035sec^{-1}$ in the upper layer, and of $.013sec^{-1}$ between the duct and the bottom. A smooth sea surface and a medium-silt bottom type were considered. Wind speed is 3 knots. The maximum number of bottom reflections is limited to one. This choice of model for the velocity profile leads to the well known problem of false caustics, producing a series of artifacts in our ambiguity plots, in the form of sudden changes of ambiguity values in the regions near the caustics.

We consider the location of a distant wideband source of unknown spectrum by a vertical linear uniform array of 5 sensors. Sensor spacing is 6 meters, and the antenna immersion (central point) is 100 meters. The source signal has a flat spectrum up to the frequency of 125 Hz (wavelength is twice the sensor spacing). Signal to noise ratio (signal power measured at the source) is 20 dB.

Fig. 1 shows the ambiguity surface over a large region, extending from the zone close to the array up to the begining of the second shadow zone. In plot (a) the source is located in the near zone, in (b) in the first shadow zone, and in (c) in the first convergence zone, always at 100 meters depth. In this plot, as well as in all subsequent plots, light areas correspond to large ambiguity, and dark regions to ambiguity values close to zero.

We see that using the complete model provides good observability conditions for all three situations considered. Note that the global structure does not change significantly over the cases considered, showing that the ambiguity level is in this case mainly dictated by the relative power of the received signal.

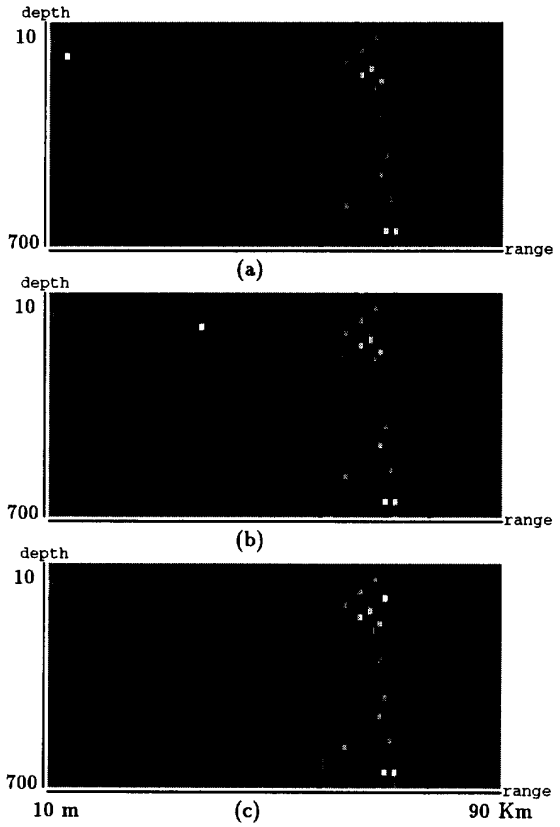

Figure 1: Ambiguity surfaces: deep ocean areas, array of 5 sensors.

In Fig. 2 we plot the ambiguity surface for the relative source/receiver geometry of Fig.1(c), but considering an array of 10 sensors (with the same total lenght, i.e., sensor spacing is now reduced to 3 meters). the two pots consider two different signal bandwidths: in (a) the source signal bandwidth is 125 Hz (as in Fig. 1) while plot (b) considers a signal with a larger bandwidth of 250 Hz.

Note that increasing the number of sensors considerably decreases the residual level of ambiguity, leading to a non-negligble improvement in observability, while bandwidth variation is not relevant for this case.

The following plot, Fig. 3 considers the effect of extending the signal bandwidth to 250 Hz for the situation of Fig.1(c). In this case, sensor spacing is no longer smaller than half wavelentgh for all frequencies of analysis. We can notice a slight change in the ambiguity structure, with slightly narrower lobes, but with an secondary peak range also slightly increased.

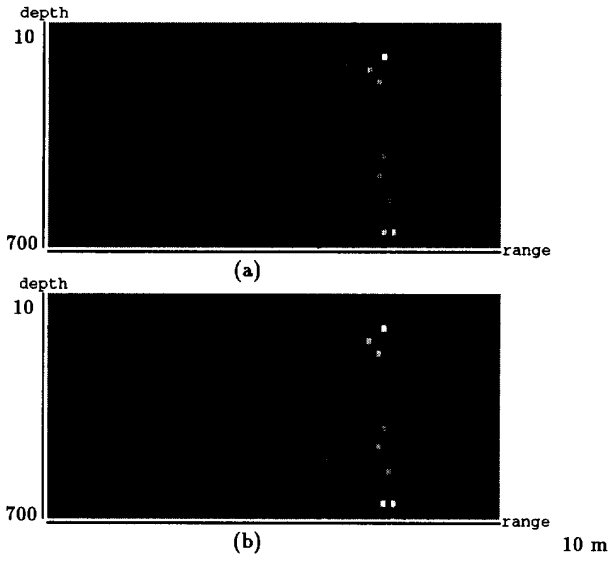

Figure 2: Ambiguity surfaces: array of 10 sensors.

This behaviour tends to accentuate with bandwidth increase.

We show in Fig.4 blow-ups of the convergence zone in Figs.1(c) and 3 that allow a more detailed comparison.

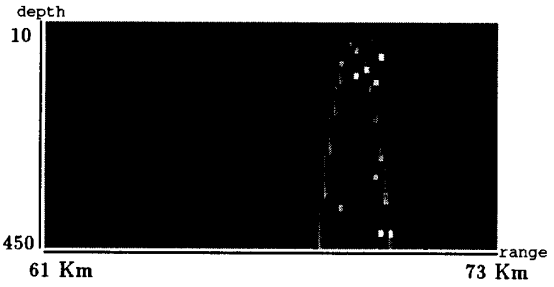

Figure 3: Increased bandwidth (250 Hz).

In Fig. 5 we study the impact of antenna immersion on source position observability. The two plots show consider the same situation as in Fig.1(c) but for an antenna located 250 meters (a) and 500 meters (b) below sea surface. We see that antenna immersion does have a profound impact on the ambiguity shape. This fact is justified by the strong vertical inhomogeneity of the received field. As the antenna is located further below surface level, the ambiguity structure becomes increasingly complex, corresponding to the presence of an increasing number of SOFAR rays.

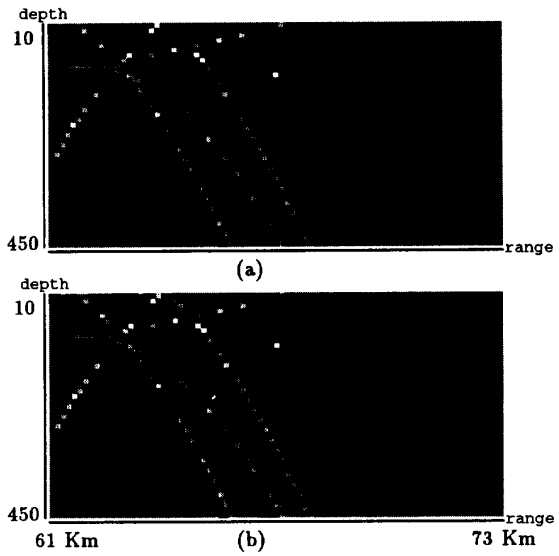

Figure 4: Detail of ambiguity surface. (a) 125 Hz (b) 250 Hz.

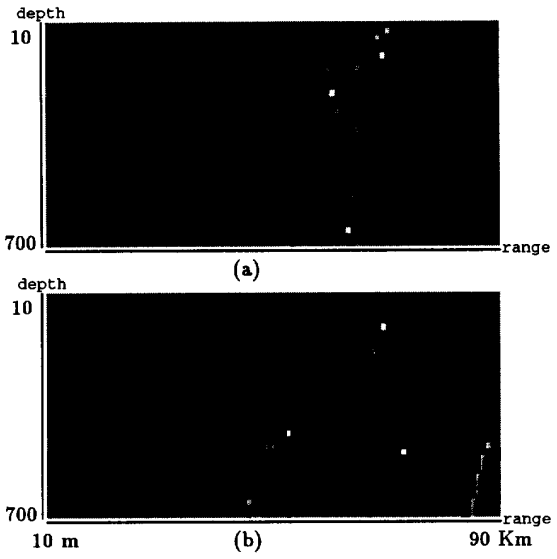

Figure 5: Ambiguity surfaces: 5 sensors.(a) antenna depth 250 m (b) antenna depth 500 m.

Next, we consider in Fig.6 the impact of source immersion. For the same scenario of Fig.1(c), we consider now placing the source at the same horizontal distance but at depth of 10 meters (a) and 300 meters (b). We see that since the field analysed by the antenna does not changes, the effect of varying source depth is almost unnoticeable. The same may not be true for situations when poorer observability conditions exist.

Finally, we show in Fig.7 the effect of increasing the signal to noise ratio to 40 dB. Only the convergence zone is ploted. Comparing Figs. 3(a) and 7 we see that no considerable improvement is observed.

4 Spatial Modeling

In this section we show plots of ambiguity surfaces considering only spatial modeling of the obsevations. As in the previous section, we consider a stochastic radiated signal of flat spectrum, observed over a vertical linear array of sensors.

The first plot considers the basic geometry of Fig.1(c). To obtain the best observability possible, we consider processing of a narrow band of the incoming wavefield (20 Hz) around 125 Hz. In plot (a) the source is in the near zone, and we see that the array offers some local resolution. For the distant source of case (b), located in the first convergence zone, the array is not able to provide information about the source location. Comparison of the sorresponding surfaces for the complete model approach reveal the potential of accurate channel modeling for improving the resovability of location mechanisms.

Figure 9 illlustrates the impact of the number of sensors of the array, ploting the ambiguity for the same situation as in plot 8(b), but for an array of 10 sensors (with the same total length). The processing band is of 20 Hz around 250 Hz, and inter-sensor spacing is 3 meters. Again, the contrast with its spatial/temporal counterpart, Fig.2(b), reveals the superiority of the complete modeling approach.

Acknowledgements

The authors would like to acknowledge the assistance of Maria Paula Santana in the development of the software package that produced the plots included in this paper.

The work of the second author was partially supported by Darpa through ONR grant N00014-91-J-1833.

References

[1] M. João D. Rendas and José M. F. Moura. Ambiguity analysis in source localization with unknown signals.

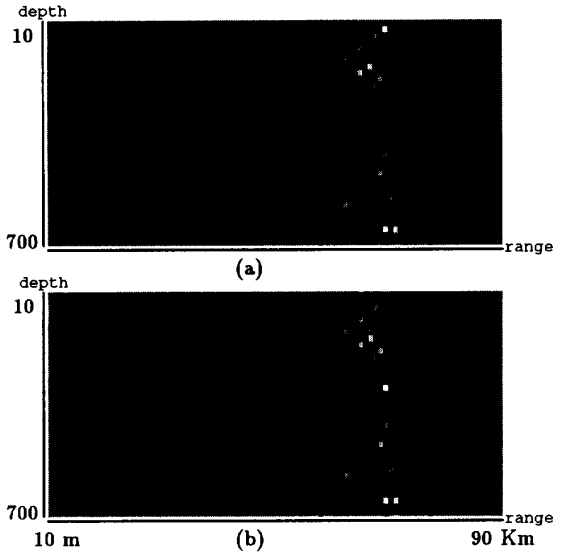

Figure 6: Ambiguity surfaces: 5 sensors.(a) source depth 10 m (b) source depth 300 m.

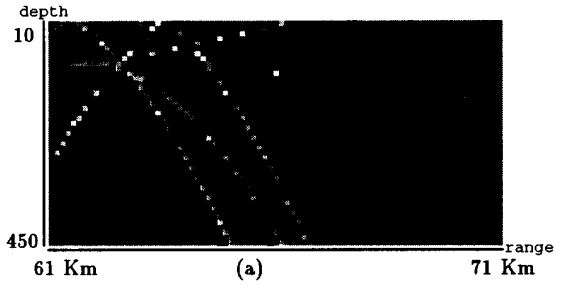

Figure 7: Variation of SNR.

In *Int. Conf. on Acoustic, Speech and Signal Processing91, Toronto, Canada*, May 1991.

[2] Maria João Rendas. *Erro e Ambiguidade em Sistemas de Localização*. PhD thesis, Instituto Superior Técnico, Lisboa, 1991.

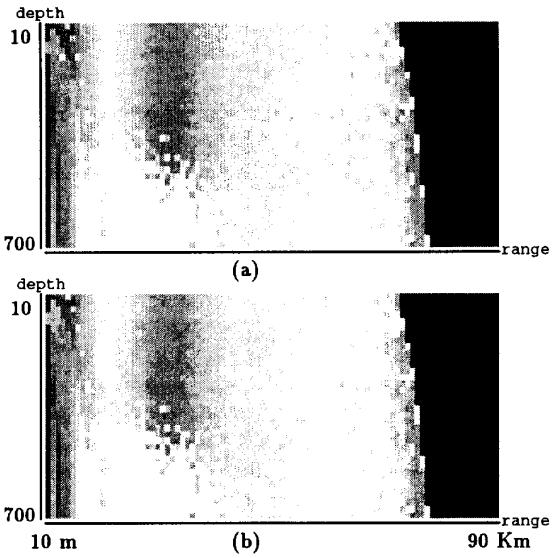

Figure 8: Spatial Modeling. (a) source in the near zone; (b) source in the first convergence zone.

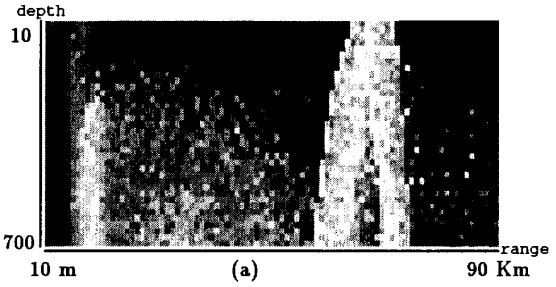

Figure 9: Spatial Modeling: increased number of sensors.